

Self-Assembly of Rationally Designed Peptides under Two-Dimensional Confinement

Lorraine Leon, Philip Logrippo, and Raymond Tu*

Chemical Engineering Department, The City College of The City University of New York, New York

ABSTRACT The rational design of interfacially confined biomolecules offers a unique opportunity to explore the cooperative relationship among self-assembly, nucleation, and growth processes. This article highlights the role of electrostatics in the self-assembly of β -sheet-forming peptides at the air-water interface. We characterize the phase behavior of a periodically sequenced sheet-forming peptide by using Langmuir techniques, Brewster angle microscopy, attenuated total reflection Fourier transform infrared spectroscopy, and circular dichroism spectroscopy. We find that peptides with an alternating binary sequence transition at high pressures from discrete circular domains to fibrous domains. The qualitative behavior is independent of surface pressure but dependent on molecular areas. In addition, thermodynamic models are employed to specifically quantify differences in electrostatics by obtaining parameters for the critical aggregation area, the limiting molecular area, and the dimensionless ratio of line tension/dipole density. Using these parameters, we are able to relate localized charge distribution to phase transitions, which will allow us to apply these molecules to examine how the dynamics of self-assembly can be directly coupled to the formation of composite nanostructures in biology.

INTRODUCTION

Rationally designed biomimetic molecules that are capable of self-assembly into nanoscale morphologies have potential use in elucidating nature's capability to process materials with exquisite precision (1–6). Peptide molecules that have the capability to self-organize at the air-water interface are particularly suited for mineralization studies because of their similarities to insoluble proteins used by nature (7) and their addressability in two dimensions. Peptides are also attractive because of the ability to iteratively control the nanoscale spatial distribution of chemical functionalities at the interface by manipulating amino-acid sequences in a rational manner (8). In contrast to previous work using polymers (9) and lipids (10) as the organic template in mineralization, peptides can be designed to assemble in particular secondary structures, namely, α -helices (11), parallel (12) or antiparallel (13) β -sheets (14), and β -hairpins (15). Formation of secondary structures introduces additional levels of control in self-assembly processes via precisely positioned hydrophobic, electrostatic, and hydrogen-bonding interactions.

Several authors have applied rationally designed peptide sequences to interfaces to control the self-assembly of well-defined secondary structures in two dimensions. Degrado and Lear (16) have worked with simple peptides consisting of a binary code. By applying a periodic sequence of only two amino acids (leucines and lysines), one can promote the formation of α -helices, β -sheets, or random coils. With regard to β -sheet structures specifically, recent studies have adopted the importance of sequence by

designing β -strands using alternating hydrophobic and hydrophilic amino acids, which can then hydrogen-bond with each other to form β -sheets. In addition, Rapaport et al. (13) have assembled β -sheets at the air-water interface and even induced long-range order in two dimensions. This has been achieved by adding Proline residues at the termini of their sequences, which disrupts hydrogen-bonding interactions leading to order in the direction perpendicular to the peptide backbone. Without these Proline residues, long-range order is only achieved via hydrogen-bonding in the direction of the peptide backbone (13). Electrostatics has been shown to be a fundamental property of self-assembly in the bulk and at the air-water interface. Studies have shown that six-residue peptides can form amyloid-like fibrils in bulk only when the net charge of the molecule is ± 1 (17). Other bulk studies have focused on electrostatics by using the same amino acids (E, A, and K) with different charge multiplets to show how a periodic β -sheet can adopt a β -hairpin structure depending on the charge distribution (18). In two dimensions, phospholipid tails have been attached to β -sheet-forming peptides showing that the non-peptide tail increases the stability of the peptide at the interface and can even facilitate the creation of multilayers (14).

The advantage of using peptidic assemblies is apparent when applied to materials processing techniques such as templated nucleation of inorganic material. Previous work using polymer matrices allowed for control over the nascent crystal properties to be achieved by varying concentration (which determines crystal size), varying ligands that attach to the polymer matrix (which determines crystal morphology), or varying the polymer matrix itself (which also controls crystal morphology) (9). Similar work using fatty acids as the organic matrix determined that the chain length of a fatty acid also had an effect on the crystal morphology (10). In

Submitted April 28, 2010, and accepted for publication August 13, 2010.

*Correspondence: tu@ccny.cuny.edu

Editor: William C. Wimley.

© 2010 by the Biophysical Society
0006-3495/10/11/2888/8 \$2.00

doi: 10.1016/j.bpj.2010.08.061

addition, work with stearic acid as the template determined that the degree of compression of the monolayer induced homogeneity of one polymorph of the resulting calcium carbonate crystals. Mann et al. (19) attributed this preference for vaterite upon compression to the decreased mobility of the organic-template. Using lipopeptide molecules, Cavalli et al. (6) were able to template indented calcium carbonate crystals, because of the ability of the lipopeptide to deform at the interface. They also attributed the nucleation of different faces of the crystal to the alignment of the lipopeptides in one direction, reorganizing the functional groups along the crystalline axis. The advantage of rationally designed peptide-based assemblies lies in the diversity of functional groups that can be introduced to the air-water interface without using entirely different materials, as is the case for polymers and fatty acids. In addition, peptide monolayers can also be compressed to achieve limited mobility and rearrangement of these diverse functional groups.

This work involves four peptide molecules that are rationally designed to form β -sheets at the air-water interface. The molecules are designed using two simple heuristics for the rational design of sheet-forming amphiphilic peptides.

First, we select amino acids that have the greatest propensity to form β -sheets, according to the particular ϕ - and ψ -angles preferred for each side group (20). The value ϕ is a torsional angle between the α -carbon and the amine, while ψ is between the α -carbon and the carbonyl group in a peptide or protein molecule. Different amino acids have different preferred ϕ - and ψ -angles because of steric hindrance and therefore have a preference toward a particular secondary structure.

Second, we apply the binary sequence periodicity associated with β -sheets, using sequences with alternating hydrophobic and hydrophilic residues (16,21).

All four sequences contain 17 amino acids and are composed of valines, glutamines, glutamic acids, histidines, and tryptophans (Fig. 1). Beta 9 and Beta 3 have the same type and number of each amino acid. They also have the same overall charge but a different charge distribution. Beta 3 has two glutamic acids separated by three amino acids (~1.4 nm), while Beta 9 has two glutamic acids separated by nine amino acids (~3.5 nm). Beta 3H and Beta 9H are identical to Beta 3 and Beta 9, except the negatively charged glutamic acids are replaced with histidines, which have pH-dependent charges. By designing peptides to have a different charge distribution, we attempt to illustrate the effect that electrostatics has on the cooperative assembly process. On the other hand, all four molecules have similar hydrogen-bonding capabilities that would favor self-assembly in the plane of the air-water interface.

The peptide molecules are characterized using Langmuir monolayer experiments, Brewster angle microscopy, circular dichroism, and attenuated total reflectance Fourier transform infrared (ATR-FTIR) spectroscopy. The Lang-

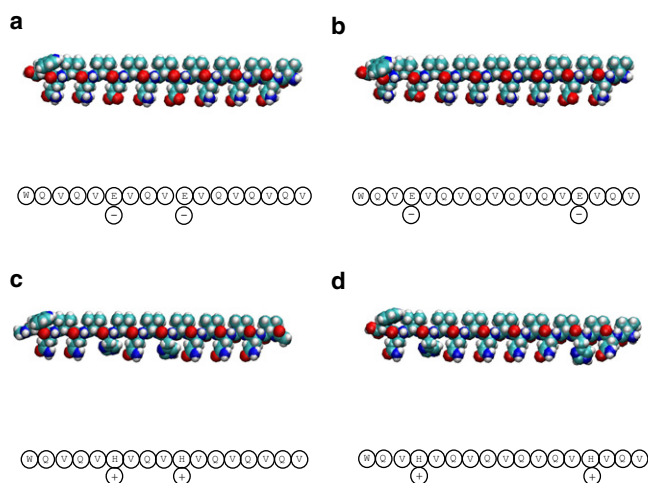


FIGURE 1 Rationally designed peptide molecules. The four peptide molecules rendered using van der Waals representation: (a) Beta 3; (b) Beta 9; (c) Beta 3H; and (d) Beta 9H.

muir trough confirms the surface activity of the molecules and shows their phase behavior by forcing them from a two-dimensional gaseous to solid phase. Using Brewster angle microscopy in conjunction with the Langmuir trough, we are able to visualize phase behavior as a function of surface pressure. Using circular dichroism and ATR-FTIR spectroscopy, we probe β -sheet formation at the air/water interface. These techniques together with a careful thermodynamic analysis allow us to quantify the role that electrostatics play during the self-assembly process in two dimensions. The molecules used in this work are selected as simplistic model molecules that can couple two known pathways for materials synthesis, self-assembly, nucleation, and growth, leading to new methods for processing of hybrid materials that possess tailored architectures at hierarchical length scales (6,22,23).

MATERIALS AND METHODS

Peptide molecules are synthesized by AnaSpec (San Jose, CA), and all have a purity of >80%. The lot numbers for Beta 3, Beta 9, Beta 3H, and Beta 9H are 69061, 69062, 69063, and 69064, respectively. The peptides are stored at -20°C . Monolayers of the peptide molecules are prepared by spreading a fresh solution of the peptide in trifluoroacetic acid/chloroform (1:9 v/v) at a concentration of 1 mg/mL. Trifluoroacetic acid, Nochromix crystals (Godax Laboratories, Takoma Park, MD), sulfuric acid (95–98%), and chloroform are obtained from Fisher Scientific (Pittsburgh, PA), and water is purified using a Millipore apparatus (Billerica, MA). Octadecyltrichlorosilane is obtained from Acros Organics (Thermo Fisher Scientific, Waltham, MA).

Langmuir trough

Surface pressure-area isotherms are obtained using a KSV minimicro trough (KSV Instruments, Helsinki, Finland). The molecules are deposited on a subphase of deionized water and are all compressed at the same speed of 5 mm/min. Monolayers of the films are transferred using vertical

deposition on a model No. 5000 trough (KSV instruments) to substrates that are hydrophobically modified using octadecyltrichlorosilane (OTS). We believe that the peptides were successfully transferred to the substrates because we obtained transfer ratios of ~ 1 . The hydrophobic modification of the substrates with octadecyltrichlorosilane was also performed using vertical deposition on a model No. 5000 trough (KSV Instruments). The procedure is discussed in detail by Kumar et al. (24) Substrates were cleaned before use by sonication in Nochromix solution (Godax Laboratories) for 30 min followed by sonication in deionized water for another 30 min (24). The Nochromix solution was prepared by dissolving the Nochromix crystals in sulfuric acid until the solution becomes transparent (24).

Brewster angle microscopy

Brewster angle microscopy images are obtained simultaneously with the surface pressure-area isotherms using an I-Elli 2000 ellipsometer/Brewster angle microscope (Nanofilm, Halcyonics, Göttingen, Germany). The resolution of the I-Elli 2000 is 1 μm in all images shown.

ATR-FTIR spectroscopy

For ATR-FTIR spectroscopy experiments, monolayers are deposited on 45° ATR Si prisms that have dimensions 50 mm \times 10 mm \times 3 mm, which are hydrophobically modified using OTS. All substrates have contact angles $>90^\circ$ before deposition of the peptide monolayer. The FTIR spectra are collected using an FTS 175 FTIR spectrometer (BioRad, Hercules, CA), configured with a horizontal ATR apparatus using a liquid-nitrogen-cooled mercury-cadmium-telluride detector. The dark count for the detector is 1×10^{-5} a.u., which is well below the integrated absorbance of the smallest peak we are considering at the lowest peptide concentration (8.775×10^{-4} a.u. for the 1701 wavenumber peak of the 5 mN/m spectra, as seen later in Fig. 4). Before obtaining the FTIR spectra of the peptide molecules, a spectra of OTS on the ATR crystal is obtained to be used as a background during the peptide spectra measurements. To verify the integrity of the peptide layer transferred to the ATR crystal, images were obtained of the peptide on a silicon substrate that was hydrophobically modified with OTS using the Brewster angle microscope. The images show similar features as the images taken at the air/water interface (data not shown).

Circular dichroism spectroscopy

For circular dichroism experiments, monolayers are deposited on quartz disks that are hydrophobically modified using OTS. All substrates have a contact angles $>90^\circ$ before deposition of the peptide monolayer. The circular dichroism spectra are collected using a model No. DSM 20 spectrophotometer (Olis, Bogart, GA). This signal/noise ratio of the data obtained was 4 at the lowest peptide concentration and 5 at the highest peptide concentration. To verify the integrity of the peptide layer transferred to the quartz disk, images were obtained of the peptide on a quartz disk that was hydrophobically modified with OTS using the Brewster angle microscope. The images show similar features as the images taken at the air/water interface (data not shown).

RESULTS AND DISCUSSION

Critical aggregation area

Fig. 2 shows the Langmuir isotherms for Beta 3, Beta 3H, Beta 9, and Beta 9H. Qualitatively, a steep liquid condensed region and a liquid expanded to liquid condensed transition occurs at very low surface pressures for all four molecules. In deionized water, both Beta 3 and Beta 9 are negatively

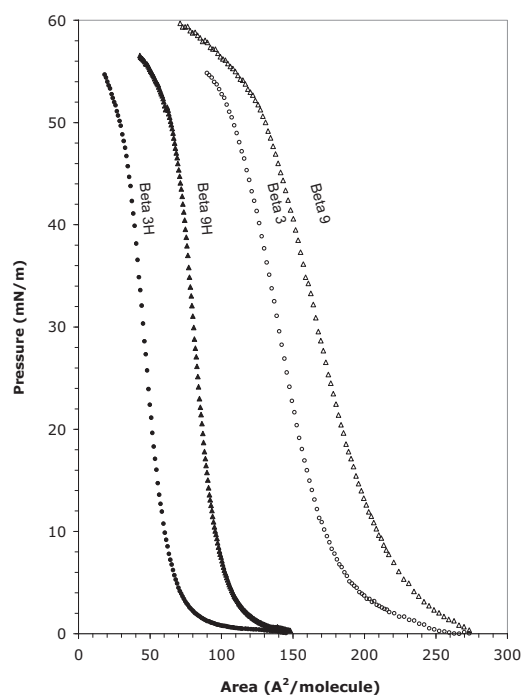


FIGURE 2 Pressure/area isotherms of the peptide molecules. The isotherms were collected at 25°C on a deionized water subphase (pH ~ 5.5) for each of the peptide molecules: Beta 9 (open triangle), Beta 3 (open circle), Beta 9H (solid triangle), and Beta 3H (solid circle).

charged, while Beta 3H and Beta 9H are neutral. This influence of charge can be seen clearly in Fig. 2 where the pressure for both the Beta 3 and the Beta 9 peptides begins to increase at much higher areas compared to Beta 3H and Beta 9H.

It is also interesting to note the difference between Beta 3 and Beta 9. Beta 9 experiences intermolecular interactions at larger areas than the Beta 3 analog. We attribute this phenomenon to the charge spacing, where more localized charges in the Beta 3 molecules allow them to arrange more compactly in a staggered fashion compared to the Beta 9 molecule where the charges are more evenly distributed. The equivalent phenomenon exists in the histidine peptides, suggesting a similar repulsion with a weaker positive charge. The outcome of these differences is quantified and visualized in subsequent sections.

In addition to single compressions, experiments have been performed using the Langmuir trough of compression and expansion cycles (data not shown). The peptides exhibit a large degree of hysteresis when comparing the compression isotherm to the expansion isotherm. We believe this hysteresis is due to the irreversible nature of assemblies that are hydrogen-bonded as observed by groups studying β -sheet assemblies at the air/water interface (25–27).

To evaluate the behavior of all four peptide molecules, their pressure/area isotherms have been quantified in terms of an equation of state. Fainerman and co-workers (28) have developed an equation that includes aggregation in

two dimensions at moderate surface pressures and extends this analysis to include interactions between molecules within an aggregate (29,30). Fainerman's analysis is derived by extending two-dimensional equations of state of gaseous monolayers, known as the Volmer equation, and includes aggregation using the chemical potential for monomers and aggregates, from Butler's equation (28). We apply the equation of Colfer et al. (15), which is an extension of Fainerman's analysis that uses relative instead of absolute surface pressure, in the analysis of our molecules. For example, the relative equation of state for the Beta 9H molecule is

$$\Pi - \Pi_{A=197} = \Pi_{rel} = \left\{ \frac{RT}{[(A - A_0)(A_C/A)]} \right\} - \left\{ \frac{RT}{[(197 - A_0)(A_C/197)]} \right\}. \quad (1)$$

The same equation was used for Beta 9, Beta 3H, and Beta 3 except for the reference area. The reference area was chosen by using the smallest area that allowed the surface pressure to remain at zero upon the addition of the peptide to the interface. The reference area was 197 Å²/molecule for Beta 3H and Beta 9H. For Beta 3 and Beta 9 the reference area was 489 Å²/molecule.

By fitting the data from the Langmuir isotherms in Fig. 2 to Eq. 1, one is able to obtain the parameters A_0 and A_C . A_C is the critical aggregation area, which is analogous to the inverse of the three-dimensional critical micelle concentration. This implies that above A_C , no aggregates are present, but below A_C , large aggregates are present (15). The term A_0 is described as the limiting molecular area or the area actually occupied by the molecule in the monolayer.

Table 1 has both values for each molecule. Comparing the A_0 values obtained, the histidine-containing peptides are smaller than the glutamic-acid-containing peptides. Additionally, in both the glutamic-acid-containing peptides and the histidine-containing peptides, the Beta 3 versions are smaller than Beta 9 versions. We also show that the A_C values for the glutamic-acid-containing peptides are much larger than that of the histidine-containing peptides. This result is nonintuitive, indicating that cohesive forces between the glutamic-acid-containing peptides are greater

than the cohesive forces for the histidine-containing peptides. However, the cohesive forces in the form of hydrogen-bond formation should be similar for each molecule. We believe that the reason the glutamic-acid-containing molecules aggregate at lower surface concentrations is that the long-range electrostatic repulsion between the molecules forces the molecules to distribute more regularly throughout the interface. On compression, this leads to the local formation of a greater number of smaller aggregates. Experiments conducted with various salt concentrations in the subphase support the hypothesis and are discussed in subsequent paragraphs.

The value of A_C for Beta 3H and Beta 9H are equivalent, indicating that aggregation occurs at the same area for both molecules. However, in the glutamic-acid-containing peptides, there is a more pronounced difference between the A_C of Beta 3 and Beta 9. Beta 9 has a lower A_C value than Beta 3. This again seems counterintuitive. At first glance one would expect that since Beta 9 possesses an A_0 value that is higher than the A_0 of Beta 3, then Beta 9 would subsequently aggregate at a larger area. However, A_C is a measure of cohesive intermolecular forces and not electrostatic repulsion. Therefore, Beta 3 with its centrally localized charge allows for hydrogen-bonding with other peptide molecules at the uncharged end of the molecule. This staggered arrangement of peptides could lead to self-assembly at lower interfacial concentrations. In contrast, Beta 9 displays its negative charge across the entire molecule and thus hydrogen-bonding between these molecules would occur only after the electrostatic repulsion of the entire molecule is overcome. It is interesting to note that the histidine molecules do not show this A_C trend. We believe that the weaker charge in these molecules makes this effect negligible.

Langmuir trough experiments were also carried out on subphases that have different concentrations of monovalent salts. Fig. 3 shows that by increasing NaCl concentration in the subphase of the Beta 3 isotherms, the curves shift to the left. This is indicative of the negative charges on the glutamic acid residues being screened and thus behaving more like their less charged counterpart Beta 3H. This is in agreement with Gouy-Chapman theory (31,32), which states that an increase in electrolyte in the subphase should increase charge screening. Similar behavior can be seen with the Beta 9 molecule (data not shown). Another way to tune the electrostatic behavior of these molecules is by varying the pH of the subphase. Additional experiments were performed on Beta 3H in which the deionized water was replaced by a pH 2 solution. The data is shown in Fig. S1 in the Supporting Material.

In Table 2, one can see the A_0 and A_C values obtained when fitting the experiments shown in Fig. 3 to the model used by Colfer et al. (15). This allows us to quantify the effect that a decreasing Debye length has on these molecules. As expected, the A_0 value for the Beta 3 molecule

TABLE 1 Values of A_0 , A_C , and λ/μ^2 for all four peptide molecules and the parameters obtained from the image analysis to find λ/μ^2

	Beta 9	Beta 3	Beta 9H	Beta 3H
A_0 (Å ² /molecule)	250.24	158.53	74.46	54.93
A_C (Å ² /molecule)	617.61	1121.46	402.14	398.22
w (μm)	0.978	1.129	1.001	0.900
Φ_v	0.133	0.172	0.092	0.078
δ (Å)	2.615	2.143	1.289	0.554
λ/μ^2	6.504	6.826	7.258	7.987

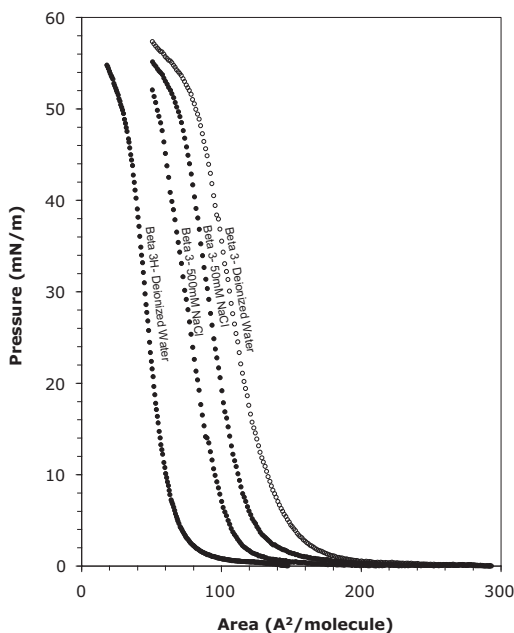


FIGURE 3 Pressure/area isotherms of Beta 3 and Beta 3H with monovalent salt. The isotherms were collected at 25°C on a deionized water subphase (pH ~ 5.5) for Beta 3 (*open circles*) and Beta 3H (*solid circles*). Isotherms were also collected for Beta 3 with a subphase of 50 mM NaCl (*light shaded circles*) and 500 mM NaCl (*dark shaded circles*).

decreases with increasing salt concentration. This indicates that the effective size of the molecule decreases as its charges are screened. The same decreasing trend follows for A_C . It is interesting to compare the A_C values for Beta 3 on a subphase of deionized water with Beta 3 on a subphase of 50 mM NaCl. The value indicates a sharp decrease in the area per molecule needed for the molecules to aggregate. This phenomenon can be explained by similar reasoning to the overall difference between the glutamic acid peptides and the histidine peptides. The A_C value for Beta 3 in a 50 mM NaCl subphase and a 500 mM subphase is similar, indicating the formation of the double layer that screens the negatively charged glutamic acid residues is close to complete at the lower concentration of NaCl.

Secondary structure

Using ATR-FTIR and circular dichroism, the secondary structure for the peptide molecules is evaluated. Both techniques indicated that the peptides are in a β -sheet confirmation at high pressures. The ATR-FTIR spectra are

TABLE 2 Values of A_0 and A_C for Beta 3 and Beta 3H on a deionized water subphase and Beta 3 on a subphase of 50 mM NaCl and 500 mM NaCl

	Beta 3	Beta 3	Beta 3	Beta 3H
Subphase	Water	50 mM NaCl	500 mM NaCl	Water
A_0 ($\text{\AA}^2/\text{molecule}$)	158.53	110.56	92.95	54.93
A_C ($\text{\AA}^2/\text{molecule}$)	1121.46	653.35	636.39	398.22

shown in Fig. 4. On increasing the surface pressure of the film from 5 mN/m to 25 mN/m, a more pronounced intermolecular weak sheet peak at 1701 cm^{-1} is observed (33). On increasing the surface pressure to 50 mN/m, the weak sheet peak is diminished, and a peak indicative of a strong sheet is observed at 1630 cm^{-1} (33). In addition to the β -sheet peaks, there is a peak present at 1655 cm^{-1} at all three pressures that is normally assigned to a random coil (33). At 5 mN/m, this peak is barely observed and it becomes more pronounced at 25 mN/m. We believe that the small peak at low pressures is due to a heterogeneous layer being present when transferring the peptide at low pressures. At 50 mN/m, this random coil peak is slightly smaller than at 25 mN/m. We believe that this diminished peak is due to a greater β -sheet content in the more compressed state. The data obtained using circular dichroism followed the same trend and can be seen in Fig. 5. At low concentrations, a peak minima indicative of a β -sheet confirmation is not evident. However, at high pressure or greater peptide concentration, it is evident that there is a minimum at $\sim 217\text{ nm}$. This is in agreement with reported values for a β -sheet structures (34). The spectra obtained for Beta 9, Beta 9H, and Beta 3 show a similar trend (data not shown).

Phase behavior

Brewster angle microscopy allows us to visualize the phase behavior of the peptide monolayers with the added benefit

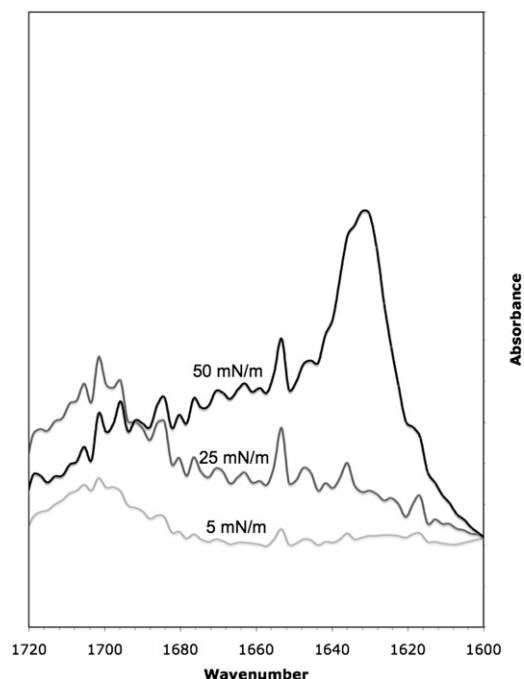


FIGURE 4 ATR-FTIR spectra confirming the presence of a β -sheet secondary structure. ATR FTIR spectra of the Beta 3H molecule was collected at varying surface pressures. The solid line is 50 mN/m, shaded line is 25 mN/m, and light shaded line is 5 mN/m.

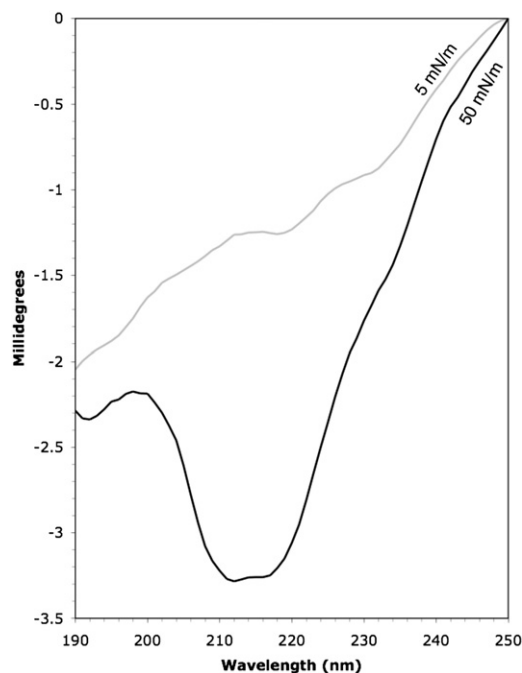


FIGURE 5 Circular dichroism spectra confirming the presence of a β -sheet secondary structure. Circular dichroism spectra of the Beta 3H molecule at a surface pressure of 5 mN/m (shaded line) and 50 mN/m (solid line).

of not having to use external probes which are needed in other techniques such as fluorescence microscopy (35). For all four peptides, one observes the emergence of circular domains between the surface pressures of 10–30 mN/m. The circular domains appear small in the image, and they tend to form a cloudy phase that occupies the entire field of view.

As the surface pressure continues to increase, there is a transition from circular domains to fibrous domains. This transition occurs between 30 and 50 mN/m with fibers being fully formed usually at 50 mN/m. Images of the fibers for each of the molecules can be seen in Fig. 6. The fibers emerge at the same surface pressure for all four molecules, which corresponds to different molecular areas as seen in Fig. 1. The fibers appear at the largest areas for Beta 9 and the smallest for Beta 3H. We also observed that the emergence of holes within the fibers occurs only in the histidine-containing molecules Beta 3H and Beta 9H, an example of which is shown in Fig. 6 *d*.

Additionally, for glutamic-acid-containing peptides, there is no phase coexistence region between the circular and fibrous transition, but coexistence has been observed for the histidine-containing peptides. We attribute this phenomenon to the difference in electrostatics between the molecules, because fiber formation should occur when the electrostatic contribution to the free energy overcomes the line tension contribution (36).

To evaluate the Brewster angle microscopy images, we use McConnell and co-worker's (37–39) theory for stripe phases occurring in monolayers. Their model balances the free energy

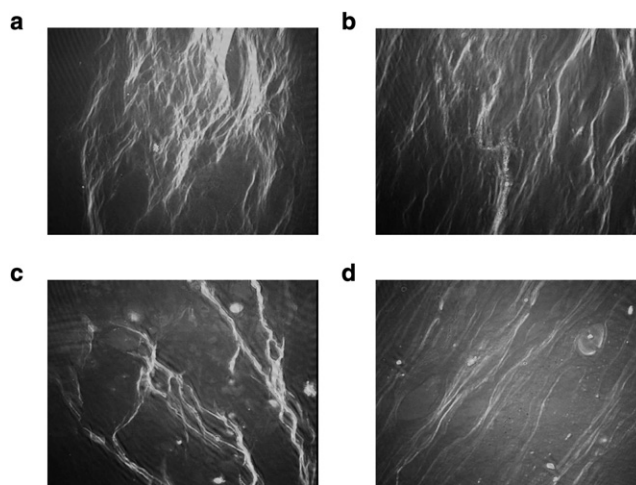


FIGURE 6 Brewster angle microscopy images of the peptide molecules assembled into fibers. The images were all taken at a surface pressure of 50 mN/m and have a width of 220 μm . (a) Beta 9; (b) Beta 3; (c) Beta 9H; and (d) Beta 3H.

contributions of line tension between domains and electrostatic interactions of the domains. They begin with the equations

$$F = \lambda p + F_{el}, \quad (2)$$

$$F_{el} = \text{const} - \frac{\mu^2}{2} \oint \oint_r \frac{1}{r} d\vec{l} d\vec{l}'. \quad (3)$$

In these equations, F is the free energy, λ is line tension, F_{el} is the electrostatic free energy, and μ is the difference in dipole density between the fluid and the solid phase. Using Eq. 2, one can explain why circular domains are observed during the compression of the molecules. At the lower pressures, line tension dominates the free energy of the system yielding circular domains. At higher pressures, there is a transition to a stripe phase for all four molecules, indicating that the electrostatic interactions are dominating the free energy. This same type of analysis explains why holes are observed in only the histidine-containing molecules because areas with few or no molecules present would occur to reduce the line tension between domains (40). By performing the integration in Eq. 3, one arrives at the following equation defining the formation of the stripe phase,

$$\bar{F}_s = 2\mu^2 \left(\frac{\phi_v}{w} \right) \left\{ \frac{\lambda}{\mu^2} - \ln \frac{w \sin(\pi \phi_v)}{2\delta \pi \phi_v} \right\}, \quad (4)$$

where ϕ_v is the solid area fraction, w is the width of the stripes, and δ is the interdipole distance. If one minimizes this equation with respect to w , one obtains

$$w = \frac{2\delta \pi e}{\sin(\pi \phi_v)} e^{\frac{\lambda}{\mu^2}}. \quad (5)$$

From our Brewster angle microscopy images, we can obtain values for w and ϕ_v . These values are obtained by using

image analysis software to determine the exact location of the fibers and calculate both the width of the fibers and the fractional area occupied. The value for δ is obtained by using the molecular area obtained from the Langmuir trough experiments at a pressure of 50 mN/m and then dividing this value by the theoretical length of these molecules, 5.0 nm. Therefore, the δ -value would be largest for Beta 9 and smallest for Beta 3H, because Beta 3H packs more tightly than the other molecules.

Rearranging Eq. 5, one obtains

$$\frac{\lambda}{\mu^2} = \ln\left(\frac{w\sin(\pi\phi_v)}{2\delta\pi\phi_v e}\right), \quad (6)$$

which gives the ratio of the line tension over the dipole density. The qualitative behavior for all four peptides is similar, showing that the binary sequence periodicity dominates interfacial self-assembly, but this dimensionless parameter gives us the ability to discern, quantitatively, the influence of electrostatics on aggregate formation sequences in terms of the forces that are dominating the free energy. Higher values of this number would indicate that line tension between boundaries is higher than electrostatic contributions to the free energy. The values for our four peptides appear in Table 1.

When we compare the values obtained, it is evident that the results are in agreement with the Langmuir trough data. The molecules with the greatest electrostatics or smallest λ/μ^2 , are the Beta 9 molecules, followed by Beta 3, Beta 9H, and then Beta 3H. When we compare the values of the histidine set to the glutamic acid set, we see that the numbers are larger for the histidine set. Comparing Beta 3 and Beta 9 in both sets of molecules also gives us greater λ/μ^2 numbers for Beta 3 as compared to Beta 9, which again supports the notion that the more localized charge in the Beta 3 molecules allows the peptides to pack more efficiently and would therefore appear to have weaker electrostatics.

CONCLUSIONS

Natural systems show an unparalleled ability to assemble composite materials across hierarchical length scales. At the heart of this materials-processing phenomenon is the ability to control self-assembly pathways. Our peptides are particularly suited to serve as an organic template capable of rearrangement into particular patterns that define mesoscale structures. We have characterized four simple rationally designed peptide molecules using tools that allow us to quantify the phase behavior and intermolecular interactions. In addition, we have applied a thermodynamic analysis for periodically sequenced peptides, resulting in a more lucid understanding of self-assembly under confinement. These tools confirm that all four variations of our

peptide are surface active, form β -sheets at the air-water interface, and form fibrillar domains at high surface concentrations when hydrogen bonding between the molecules dominates the free energy. Interestingly, we observe that charge leads to the formation of distributed aggregates at lower surface concentrations as spatially localized charge influences the packing of peptides at the interface. This analysis allows us to now explore the nonequilibrium cooperative relationship between self-assembly and composite biomaterials processing.

SUPPORTING MATERIAL

One figure is available at [http://www.biophysj.org/biophysj/supplemental/S0006-3495\(10\)01057-X](http://www.biophysj.org/biophysj/supplemental/S0006-3495(10)01057-X).

The authors acknowledge financial support from the Air Force Office of Scientific Research (grant No. FA9550-08-1-0041). P.L. acknowledges the National Science Foundation for support through the Research Experiences for Undergraduates (grant No. 0648788).

REFERENCES

- Gazit, E. 2007. Self-assembled peptide nanostructures: the design of molecular building blocks and their technological utilization. *Chem. Soc. Rev.* 36:1263–1269.
- Langer, R., and D. A. Tirrell. 2004. Designing materials for biology and medicine. *Nature.* 428:487–492.
- Rajagopal, K., and J. P. Schneider. 2004. Self-assembling peptides and proteins for nanotechnological applications. *Curr. Opin. Struct. Biol.* 14:480–486.
- Sarikaya, M., C. Tamerler, ..., F. O. Baneyx. 2004. Materials assembly and formation using engineered polypeptides. *Annu. Rev. Mater. Res.* 34:373–408.
- Zhang, S. 2002. Emerging biological materials through molecular self-assembly. *Biotechnol. Adv.* 20:321–339.
- Cavalli, S., D. C. Popescu, ..., A. Kros. 2006. Self-organizing β -sheet lipopeptide monolayers as template for the mineralization of CaCO_3 . *Angew. Chem. Int. Ed. Engl.* 45:739–744.
- Weiner, S., and W. Traub. 1980. X-ray diffraction study of the insoluble organic matrix of mollusk shells. *FEBS Lett.* 111:311–316.
- Tu, R. S., and M. Tirrell. 2004. Bottom-up design of biomimetic assemblies. *Adv. Drug Deliv. Rev.* 56:1537–1563.
- Bianconi, P. A., J. Lin, and A. R. Strzelecki. 1991. Crystallization of an inorganic phase controlled by a polymer matrix. *Nat. Lett.* 349: 315–317.
- Loste, E., E. Diaz-Marti, ..., F. Meldrum. 2003. Study of calcium carbonate precipitation under a series of fatty acid Langmuir monolayers using Brewster angle microscopy. *Langmuir.* 19:2830–2837.
- Jain, V., A. Jimenez, ..., R. S. Tu. 2008. Dynamic surface activity by folding and unfolding an amphiphilic α -helix. *Langmuir.* 24: 9923–9928.
- Sneer, R., M. J. Weygand, ..., H. Rapaport. 2004. Parallel β -sheet assemblies at interfaces. *ChemPhysChem.* 5:747–750.
- Rapaport, H., K. Kjaer, ..., D. Tirrell. 2000. Two-dimensional order in-sheet peptide monolayers. *J. Am. Chem. Soc.* 122:12523–12529.
- Cavalli, S., J. W. Handgraaf, ..., A. Kros. 2006. Two-dimensional ordered β -sheet lipopeptide monolayers. *J. Am. Chem. Soc.* 128:13959–13966.
- Colfer, S., J. Kelly, and E. Powers. 2003. Factors governing the self-assembly of a β -hairpin peptide at the air-water interface. *Langmuir.* 19:1312–1318.

16. DeGrado, W. F., and J. D. Lear. 1985. Induction of peptide conformation at apolar/water interfaces. 1. A study with model peptides of defined hydrophobic periodicity. *J. Am. Chem. Soc.* 107:7684–7689.
17. López de la Paz, M., K. Goldie, ..., L. Serrano. 2002. De novo designed peptide-based amyloid fibrils. *Proc. Natl. Acad. Sci. USA.* 99:16052–16057.
18. Jun, S., Y. Hong, ..., P. Chen. 2004. Self-assembly of the ionic peptide EAK16: the effect of charge distributions on self-assembly. *Biophys. J.* 87:1249–1259.
19. Mann, S., B. Heywood, ..., J. Birchall. 1988. Controlled crystallization of CaCO₃ under stearic acid monolayers. *Nature.* 334:692–695.
20. Chou, P. Y., and G. D. Fasman. 1974. Prediction of protein conformation. *Biochemistry.* 13:222–245.
21. Xiong, H., B. L. Buckwalter, ..., M. H. Hecht. 1995. Periodicity of polar and nonpolar amino acids is the major determinant of secondary structure in self-assembling oligomeric peptides. *Proc. Natl. Acad. Sci. USA.* 92:6349–6353.
22. Xu, A. W., Y. R. Ma, and H. Colfen. 2007. Biomimetic mineralization. *J. Mater. Chem.* 17:415–449.
23. Mann, S. 2009. Self-assembly and transformation of hybrid nano-objects and nanostructures under equilibrium and non-equilibrium conditions. *Nat. Mater.* 8:781–792.
24. Kumar, V., S. Krishnan, ..., A. Couzis. 1998. Measurement of infrared molar absorptivity of a surfactant adsorbed onto a solid substrate over a wide range of surface concentrations using octadecyltrichlorosilane Langmuir-Blodgett transferred films. *J. Phys. Chem. B.* 102:3152–3159.
25. Reda, T., H. Hermel, and H. D. Hoeltje. 1996. Compression/expansion hysteresis of poly (L-glutamic acid) monolayers spread at the air/water. *Langmuir.* 12:6452–6458.
26. Triulzi, R., C. Li, ..., R. Leblanc. 2007. A two-dimensional approach to study amyloid β -peptide fragment (25–35). *J. Phys. Chem. C.* 111:4661–4666.
27. Parazak, D., J. Uang, ..., K. Stine. 1994. Fluorescence microscopy study of chiral discrimination in Langmuir monolayers of N-acylvaline and N-acylalanine amphiphiles. *Langmuir.* 10:3787–3793.
28. Fainerman, V., D. Vollhardt, and V. Melzer. 1996. Equation of state for insoluble monolayers of aggregating amphiphilic molecules. *J. Phys. Chem.* 100:15478–15482.
29. Fainerman, V., and D. Vollhardt. 1999. Equations of state for Langmuir monolayers with two-dimensional phase transitions. *J. Phys. Chem. B.* 103:145–150.
30. Vollhardt, D., V. B. Fainerman, and S. Siegel. 2000. Thermodynamic and textural characterization of DPPG phospholipid monolayers. *J. Phys. Chem. B.* 104:4115–4121.
31. Aveyard, R., and D. A. Haydon. 1973. *An Introduction to the Principles of Surface Chemistry.* Cambridge University Press, Cambridge, UK.
32. Israelachvili, J. 1991. *Intermolecular and Surface Forces.* Academic Press, New York.
33. Hu, X., D. Kaplan, and P. Cebe. 2006. Determining β -sheet crystallinity in fibrous proteins by thermal analysis and infrared spectroscopy. *Macromolecules.* 39:6161–6170.
34. Johnson, Jr., W. C. 1988. Secondary structure of proteins through circular dichroism spectroscopy. *Annu. Rev. Biophys. Biophys. Chem.* 17:145–166.
35. Lheveder, C., S. Hénon, ..., J. Meunier. 1998. A new Brewster angle microscope. *Rev. Sci. Instrum.* 69:1446–1450.
36. Seul, M., and D. Andelman. 1995. Domain shapes and patterns: the phenomenology of modulated phases. *Science.* 267:476–483.
37. McConnell, H. M. 1989. Theory of hexagonal and stripe phases in monolayers. *Proc. Natl. Acad. Sci. USA.* 86:3452–3455.
38. McConnell, H. M. 1991. Structures and transitions in lipid monolayers at the air-water interface. *Annu. Rev. Phys. Chem.* 42:171–195.
39. McConnell, H. M., and V. T. Moy. 1988. Shapes of finite two-dimensional lipid domains. *J. Phys. Chem.* 92:4520–4525.
40. Kohlstedt, K., G. Vernizzi, and M. Cruz. 2009. Surface patterning of low-dimensional systems: the chirality of charged fibers. *J. Phys. Condens. Matter.* 21:424114.